ACS APPLIED MATERIALS & INTERFACES

Research Article

www.acsami.org

Facile One-Step Synthesis of Three-Dimensional Pd–Ag Bimetallic Alloy Networks and Their Electrocatalytic Activity toward Ethanol Oxidation

Shaofang Fu,[†] Chengzhou Zhu,[†] Dan Du,[†] and Yuehe Lin*[,†,‡]

[†]Department of Mechanical and Materials Engineering, Washington State University, Pullman, Washington 99164, United States

[‡]Pacific Northwest National Laboratory, Richland, Washington 99352, United States

Supporting Information

ABSTRACT: The three-dimensional palladium networks and palladium–silver bimetallic alloy networks were synthesized at room temperature on a large scale using a rapid and simple strategy. The results revealed that the morphology of the networks is not affected by the composition. We demonstrated that the as-prepared unsupported networks exhibited excellent electrochemical activity and stability toward ethanol oxidation reaction in alkaline media due to the formation of palladium–silver alloys as well as the porous nanostructures. The results indicate that the well-defined three-dimensional palladium–silver bimetallic alloy networks are promising catalysts for fuel cells.

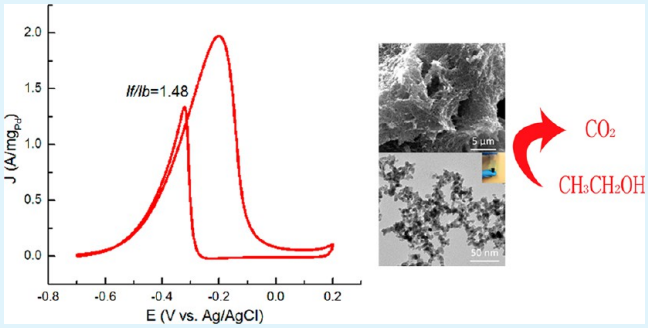

KEYWORDS: *Pd, bimetallic alloy, three-dimensional networks, fuel cell, ethanol oxidation reaction*

1. INTRODUCTION

Noble metals, such as platinum (Pt), palladium (Pd), and gold (Au), have been used in various areas for decades, including fuel cell catalysts,[1,2] cell imaging,[3,4] surface-enhanced Raman spectroscopy (SERS),[5−7] biosensing,[8] and drug delivery.[9,10] Particularly, the rational design of noble metal nanostructures with favorable size, shape, and composition provides wide opportunities to construct advanced electrocatalysts in fuel cells with high activity and stability.[11,12] For instance, Pd presents high catalytic activity and stability for ethanol oxidation reaction (EOR) in alkaline solutions even though it has no electrocatalytic activity in acid type direct ethanol fuel cells (DEFCs).[13,14] However, the efficiency and activity of Pd-based catalysts are still the main challenges for DEFC applications. To overcome these problems, a number of strategies have been explored, including alloying with other nonprecious metals and adjusting morphologies of the nanostructures.[12,15−17] To this end, silver (Ag), copper (Cu), ruthenium (Ru), and tin (Sn) have been used to form alloys with Pd, which presented good catalytic activity toward EOR.[14,18−22] For example, Ding et al. synthesized Pd–Sn hierarchical alloy nanosheet dendrites by an electrodeposition approach, which exhibited high electrocatalytic activity and superior long-term cycle stability toward EOR.[23] The addition of the nonprecious metal not only efficiently enhances the electrochemical performance of the EOR but also greatly decreases the cost of the electrocatalysts.

On the other hand, specific structures, such as three-dimensional (3D) noble metal networks (NWs), nanoflowers, nanoneedles, nanodendrites, or core–shells, have significant effects on the properties of the materials.[16,24−27] Among them, 3D NWs have attracted many interests in the area of sensors,[19] drug delivery,[28] and fuel cells,[22] due to their high surface area, low density, and special electrical properties.[19] For the fuel cell application, the 3D NWs materials can serve as catalysts themselves, which have shown high activities and satisfactory stability in comparison to commercial carbon supported Pt catalyst. This type of nanostructures is characterized by contiguous material that is effectively presintered, thus minimizing loss of electrochemical surface area (ECSA) due to an agglomeration pathway. At the same time, the elimination of the carbon support would allow for a thinner electrode catalyst layer and for improved mass transport and Pt utilization within the catalyst layer because the catalyst layer would be in direct contact with the gas diffusion layer.[29−31] In this study, we synthesized 3D Pd NWs and Pd–Ag bimetallic alloy networks (BANWs) on a large scale. Compared with other synthesis strategies, the Pd–Ag BANWs were prepared by a rapid aqueous solution method without formation of silver chloride (AgCl).[26,32,33] The as-prepared NWs can be directly utilized as unsupported electrocatalyst and exhibited enhanced activity and stability on EOR in alkaline solutions compared with commercial palladium/carbon (Pd/C) catalyst. Therefore, it is

Received: March 4, 2015
Accepted: June 8, 2015
Published: June 8, 2015

DOI: 10.1021/acsami.5b01963
ACS Appl. Mater. Interfaces 2015, 7, 13842−13848

expected that these novel 3D porous nanostructures hold great promise in fuel cells and other electrochemical applications.

2. EXPERIMENTAL SECTION

2.1. Chemicals and Reagents. Sodium borohydride ($NaBH_4$, 98%, powder), silver nitrate ($AgNO_3$, 99.9+%), and palladium on activated carbon powder (20% Pd loading, nominally 57.05% water wet) were purchased from Alfa Aesar. Potassium hydroxide (KOH, reagent grade) was obtained from Amresco. Palladium(II) nitrate hydrate ($Pd(NO_3)_2{\cdot}xH_2O$, Pd ~ 41.9%, Pd 99.9%) was bought from Strem Chemicals. Ethanol 200 proof (CH_3CH_2OH) was purchased from Decon Laboratories.

2.2. Characterization. Transmission electron microscopy (TEM) images were obtained by a Philips CM200 UT (Field Emission Instruments, USA). FEI Sirion field emission scanning electron microscope (FESEM) was used for imaging and energy-dispersive X-ray analysis (EDX). X-ray diffraction (XRD) characterization was carried out by a Rigaku Miniflex 600. The tube was operated at 40 kV accelerating voltage and 15 mA current.

2.3. Synthesis of 3D Pd NWs and Pd−Ag BANWs. 3D Pd−Ag BANWs were synthesized using a simple aqueous solution method. Briefly, 1 mL of metal precursor aqueous solution containing $Pd(NO_3)_2{\cdot}xH_2O$ and $AgNO_3$, with a total metal ions concentration of 0.1 M, was injected into $NaBH_4$ solution (0.1 M, 5 mL). The mixture was stirred until the solution became colorless. The black products were then washed with DI water, followed by drying at room temperature. As a comparison, pure 3D Pd NWs were synthesized using the same method. The final products were denoted as Pd, $Pd_{67}Ag_{33}$, $Pd_{50}Ag_{50}$, and $Pd_{33}Ag_{67}$, respectively, according to the different compositions.

2.4. Electrochemical Experiments. The Pd NWs, Pd−Ag BANWs, and commercial Pd/C catalysts (0.1 M with respect to total metal ions) were obtained by dissolving the catalysts into deionized water. Then, the catalysts with a Pd loading of 1.25 μg were dropped onto the polished and cleaned glassy carbon electrode (GCE, 3 mm in diameter) surface and dried at 60 °C. After that, 2.5 μL of 0.05% nafion was covered on the surface and dried under the same condition.

The electrochemical measurements were conducted on an electrochemical workstation (CHI 630E) coupled with a three-electrode system. A Pt wire and a Ag/AgCl electrode filled with saturated KCl aqueous solution were used as the counter electrode and reference electrode, respectively.

3. RESULTS AND DISCUSSION

3.1. Characterization of 3D Pd NWs and Pd−Ag BANWs. The morphology of Pd NWs (Figure 1a) and Pd−Ag BANWs (Figure 1b−d) were characterized by scanning electron microscopy (SEM), which confirms the formation of the foam-like 3D NWs by a simple aqueous method. With a higher magnification, the porous structure is clearly observed, as shown in Figure 1d. The similar morphology for each sample indicates that the ratio of Pd to Ag does not have much effect on the structure of the NWs.

The NWs structures of Pd, $Pd_{67}Ag_{33}$, and $Pd_{50}Ag_{50}$ were further characterized by transmission electron microscopy (TEM), as shown in Figure 2. All the 3D NWs presented a similar structure, where the networks are composed of fused nanoparticles. The diameters of nanoparticles in Pd NWs and $Pd_{67}Ag_{33}$, and $Pd_{50}Ag_{50}$ BANWs are 5.9, 5.7, and 6.0 nm, respectively (Figure S1a−c, Supporting Information), which was measured by Nano Measure Software. This result confirms that the composition does not have an effect on the morphology of the NWs. The inset in Figure 2a shows the digital photograph of 3D Pd−Ag BANWs, which demonstrates that the sample with 3D networks could be produced on a large

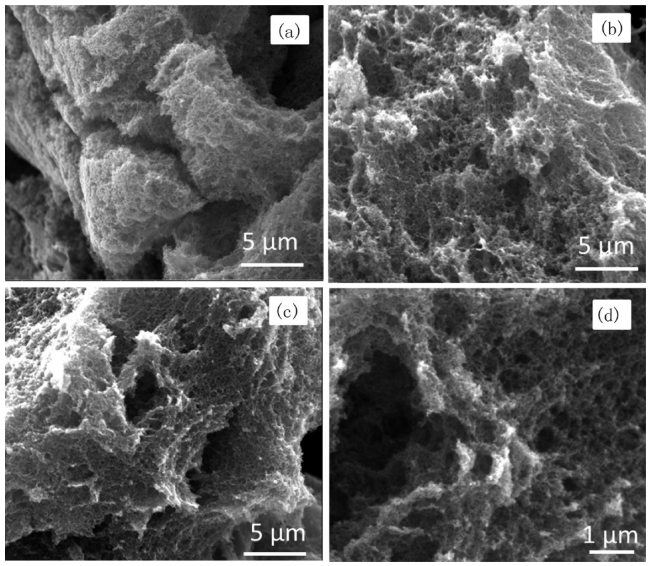

Figure 1. SEM images of as-prepared 3D Pd NWs (a) and $Pd_{67}Ag_{33}$ (b) and $Pd_{50}Ag_{50}$ (c, d) BANWs.

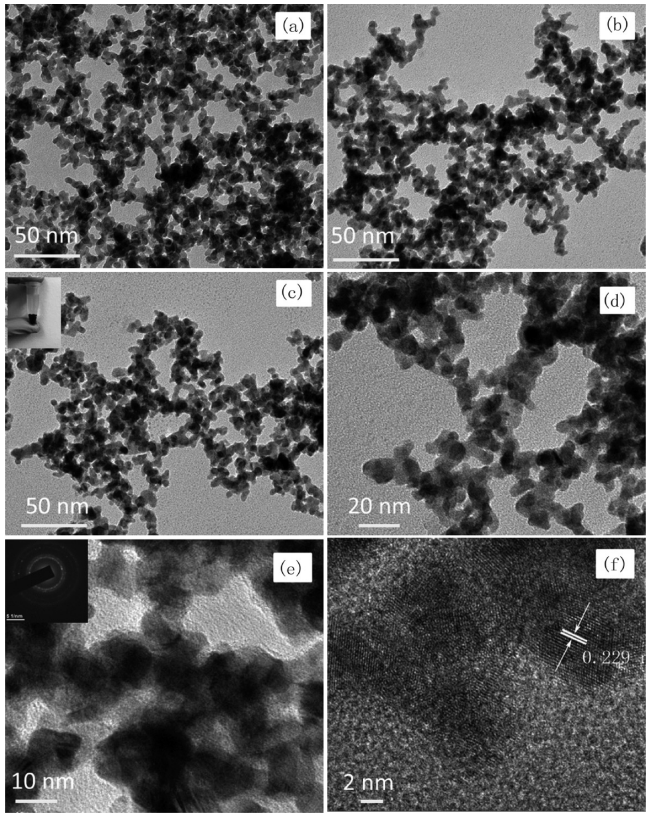

Figure 2. TEM images of Pd NWs (a) and $Pd_{67}Ag_{33}$ (b) and $Pd_{50}Ag_{50}$ (c, d, e) BANWs. Inset in (c) is the digital photograph of Pd−Ag BANWs. Inset in (e) is the SEAD pattern of $Pd_{50}Ag_{50}$ BANWs. (f) HRTEM image of $Pd_{50}Ag_{50}$ BANWs.

scale. The polycrystalline structure of $Pd_{50}Ag_{50}$ BANWs was further demonstrated by the selected area electron diffraction (SAED) pattern, as shown in Figure 2e, inset. It confirmed that the Pd−Ag NWs were formed by the fusion of nanoparticles. The structure of a $Pd_{50}Ag_{50}$ BANW individual nanoparticles was characterized by high-resolution transmission electron microscopy (HRTEM), as shown in Figure 2f. The image

DOI: 10.1021/acsami.5b01963
ACS Appl. Mater. Interfaces 2015, 7, 13842−13848

reveals that the measured interplanar spacing is around 0.229 nm. This value corresponds to the (111) lattice plane of the Pd−Ag alloy nanostructure.

To analyze the composition of 3D $Pd_{67}Ag_{33}$ and $Pd_{50}Ag_{50}$ BANWs, energy-dispersive X-ray (EDX) spectroscopy was used (Figure 3d and Figure S2d, Supporting Information). The

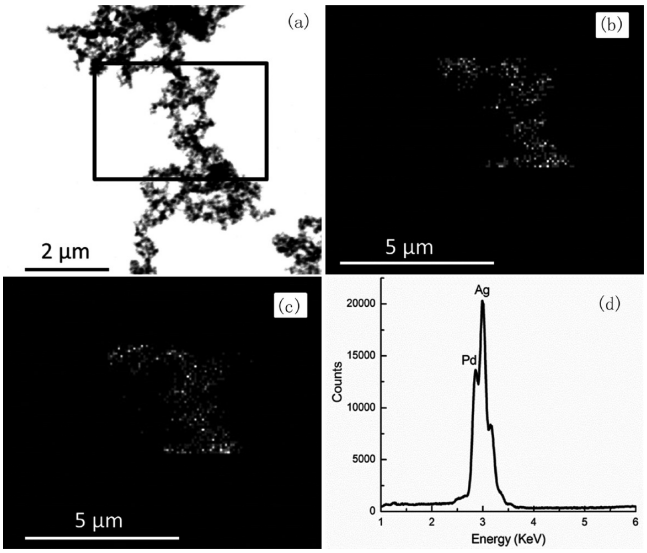

Figure 3. (a) TEM image of 3D $Pd_{50}Ag_{50}$ BANWs and related element mapping of Pd (b) and Ag (c). (d) EDX spectrum of $Pd_{50}Ag_{50}$ BANWs.

peaks representing Pd and Ag shown on the spectra confirm the presence of these two elements in the NWs. On the basis of EDX results, the ratios of Pd to Ag are 62:38 and 47:53 for $Pd_{67}Ag_{33}$ and $Pd_{50}Ag_{50}$ BANWs, respectively, which are close to 67:33 and 50:50. It is clear that the precursors added can be totally reduced in the presence of a strong reducing agent. Moreover, Figure 3 and Figure S2 show the TEM images and related element mapping images of Pd and Ag for $Pd_{67}Ag_{33}$ and $Pd_{50}Ag_{50}$ BANWs. The maps confirm the formation of Pd−Ag alloys, which are uniformly distributed all over the 3D NWs.

The X-ray diffraction (XRD) patterns of Pd NWs and Pd−Ag BANWs reveal their fcc structures, as shown in Figure 4a. For the Pd NWs, the peaks observed at 2θ = 40.08, 46.5, 68, 81.9, and 86.42° correspond to (111), (200), (220), (311), and (222) planes. For Pd−Ag BANWs, these peaks shift to a smaller angle because of the presence of Ag. The peak positions of $Pd_{67}Ag_{33}$ and $Pd_{50}Ag_{50}$ are located between Pd (green) and Ag (red) peaks, indicating the alloy formation between Pd and Ag. The bimetallic Pd−Ag nanoparticles' size can be calculated according to Scherrer equation[34]

$$L = \frac{0.9\lambda_{K\alpha 1}}{B_{2\theta}\cos\theta_{max}}$$

where L is the size of Pd−Ag nanoparticles. $\lambda_{K\alpha 1}$ is the X-ray wavelength (λ = 0.154 nm). $B_{2\theta}$ is the half-peak width. θ_{max} is the Bragg angle. The calculated nanoparticle sizes of Pd NWs and $Pd_{67}Ag_{33}$ and $Pd_{50}Ag_{50}$ BANWs are 5.67, 6.12, and 6.38 nm, which agree with the TEM results very well.

The presence of Pd and Ag in $Pd_{67}Ag_{33}$ and $Pd_{50}Ag_{50}$ was further confirmed by X-ray photoelectron spectroscopy (XPS). Figure 4b shows the Pd XPS spectra for Pd NWs and $Pd_{67}Ag_{33}$ and $Pd_{50}Ag_{50}$ BANWs. It reveals that the peak positions for Pd ($3d_{5/2}$) and Pd ($3d_{3/2}$) in BANWs negatively shift relative to that of Pd NWs. This shift should be attributed to the alloy formation between Pd and Ag in $Pd_{67}Ag_{33}$, and $Pd_{50}Ag_{50}$ BANWs. Figure 4c shows the deconvolution of Pd 3d spectra for $Pd_{50}Ag_{50}$ BANWs. It presents two sets of peaks. One set shows Pd ($3d_{5/2}$) at 335.2 eV and Pd ($3d_{3/2}$) at 340.5 eV, corresponding to Pd (0). The other set presents Pd ($3d_{5/2}$) at 336.9 eV and Pd ($3d_{3/2}$) at 342.4 eV, which are assigned to Pd (II).[35] The deconvolution results reveal that Pd (0) is the dominant composition in $Pd_{50}Ag_{50}$ BANWs. The XPS quantification results reveal that the ratios between Pd and Ag are 49.21:50.79 and 38.71:61.29 for $Pd_{67}Ag_{33}$ and $Pd_{50}Ag_{50}$, respectively, which are much lower than the expected values. It is noted that the outer surfaces of these nanostructures are enriched with Ag, which is attributed to the higher reduction potential of Pd^{2+} compared to that of Ag^{+}.

3.2. Ethanol Oxidation with 3D Pd NWs and Pd−Ag BANWs. The electrocatalytic activities of 3D Pd NWs and Pd−Ag BANWs were studied by cyclic voltammetry (CV) from −0.7 to 0.2 V with the same Pd loading. Figure 5a shows the typical CV curves of Pd-based 3D NWs as well as commercial Pd/C catalysts in N_2-saturated 1 M KOH solution. All the samples present reduction peaks of palladium oxides between −0.33 and −0.25 V in the negative scan. For Pd NWs and $Pd_{67}Ag_{33}$, and $Pd_{50}Ag_{50}$ BANWs, it reveals that palladium oxides were reduced at relatively lower potential in the sample with higher Ag concentration. Additionally, the reduction peak current increased with the increase in the Ag concentration.

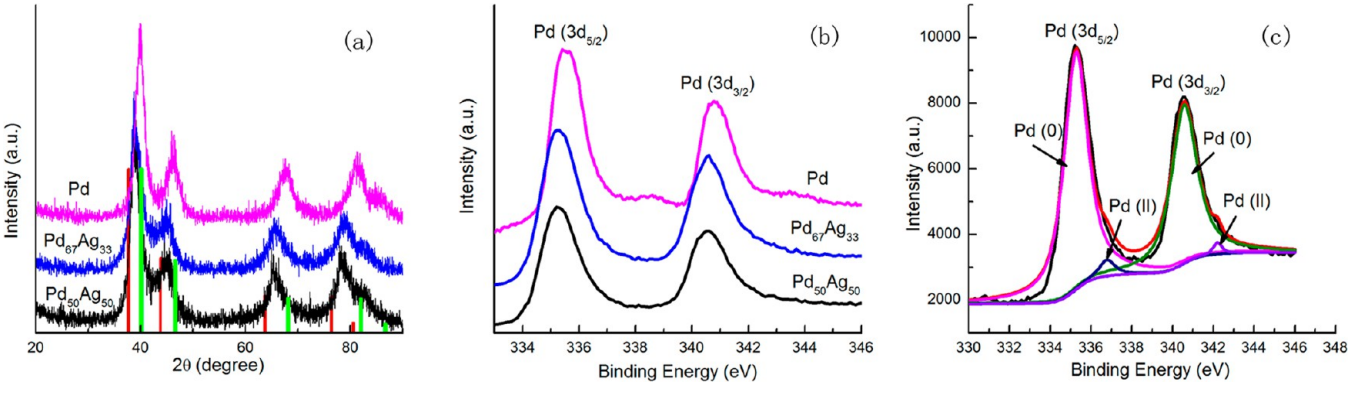

Figure 4. (a) XRD patterns of Pd NWs and $Pd_{67}Ag_{33}$ and $Pd_{50}Ag_{50}$ BANWs. JADE database peak positions for Pd (green) and Ag (red). (b) Pd XPS spectra of Pd NWs and $Pd_{67}Ag_{33}$ and $Pd_{50}Ag_{50}$ BANWs. (c) Deconvolution of Pd XPS spectra for $Pd_{50}Ag_{50}$ BANWs.

DOI: 10.1021/acsami.5b01963
ACS Appl. Mater. Interfaces 2015, 7, 13842−13848

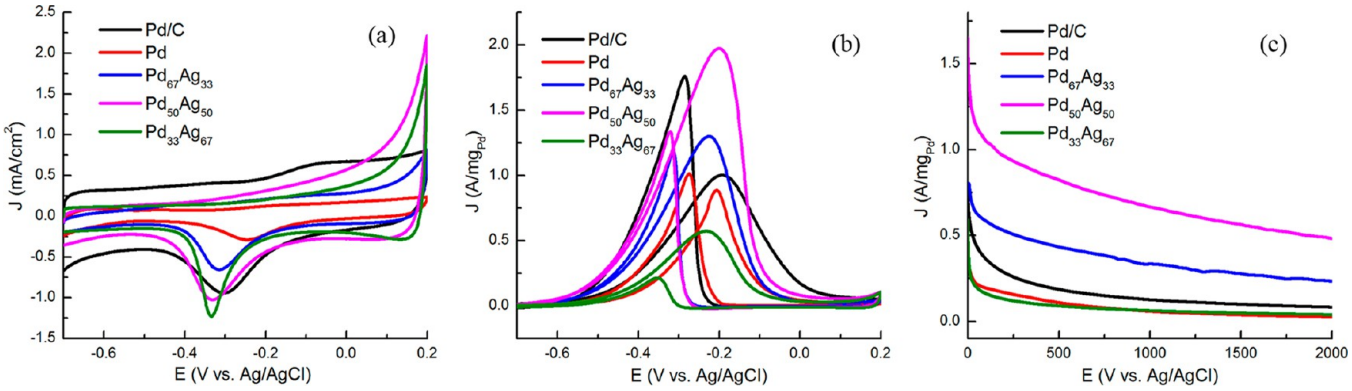

Figure 5. CV curves of Pd NWs, $Pd_{67}Ag_{33}$, $Pd_{50}Ag_{50}$, and $Pd_{33}Ag_{67}$ BANWs, and Pd/C catalysts in N_2-saturated 1 M KOH (a) and 1 M KOH + 1 M CH_3CH_2OH solution (b) at a scan rate of 50 mV/s. (c) Chronoamperometric curves of Pd NWs, $Pd_{67}Ag_{33}$, $Pd_{50}Ag_{50}$, and $Pd_{33}Ag_{67}$ BANWs, and Pd/C catalysts in N_2-saturated 1 M KOH + 1 M CH_3CH_2OH solution at an electrode potential of −0.3 V.

Table 1. Electrochemical Parameters of Commercial Pd/C, Pd NWs, and Pd−Ag BANWs

	ECSA (m^2/g_{Pd})	onset potential (V)	peak current (A/mg_{Pd})	I_f/I_b
Pd/C	24.38	−0.46	1.01	0.57
Pd	10.55	−0.39	0.89	0.88
$Pd_{67}Ag_{33}$	19.48	−0.47	1.30	1.1
$Pd_{50}Ag_{50}$	32.81	−0.50	1.97	1.48
$Pd_{33}Ag_{67}$	23.23	−0.45	0.57	2.59

These phenomena are attributed to the presence of Ag in Pd−Ag alloys. However, this trend does not maintain as the ratio between Pd and Ag increased to 1:2. $Pd_{33}Ag_{67}$ BANWs present the highest reduction peak, while the peak potential is almost same as that of $Pd_{50}Ag_{50}$ BANWs. In the positive scan, OH^- was adsorbed onto the surface of catalysts. An obvious onset potential could be observed on $Pd_{67}Ag_{33}$, $Pd_{50}Ag_{50}$, and $Pd_{33}Ag_{67}$ BANWs, which is associated with the alloy nanostructures in these three samples. Namely, the Pd−Ag alloy is favorable for the adsorption of OH^-. In comparison with $Pd_{67}Ag_{33}$ and $Pd_{33}Ag_{67}$ BANWs, $Pd_{50}Ag_{50}$ shows a more negative onset potential, indicating the easier adsorption of OH^- on the surface.[36]

According to the CV curves in Figure 5a, the corresponding ECSA of each catalyst was calculated by quantification of the electric charges associated with the reduction of PdO,[37] as shown in the following equation[38]

$$\mathrm{ECSA} = \frac{Q}{m \times C \times v}$$

where Q is the charge for PdO reduction on the surface, which can be obtained from the area integral of Figure 5a. m is the mass of Pd (1.25 μg). C is the charge required to reduce the layer of PdO (420 $\mu C/cm^2$). v is the scan rate, which is 50 mV/s. The calculated ECSA is listed in Table 1. It has been demonstrated that ECSA dominates the electrocatalytic activity of catalyst materials. Higher ECSA contributes to an increase of EOR activity and thus an increase of the overall fuel cell performance.[39] The specific ECSA of the $Pd_{50}Ag_{50}$ BANWs (32.81 m^2/g_{Pd}) is highest among the synthesized samples, which is even higher than that of commercial Pd/C catalyst (24.38 m^2/g_{Pd}). It should be noted that the ECSA is increasing with the increase of Ag concentration within a certain range. However, the further increase of the Ag:Pd ratio shows an inhibiting effect on the ECSA.

With the addition of 1 M ethanol, the 3D Pd NWs and Pd−Ag BANWs exhibit electrochemical activity toward EOR in alkaline media, as shown in Figure 5b. All the samples display a typical current peak in the forward scan, representing the oxidation of ethanol. The onset potential and peak current of each catalysts are summarized in Table 1. A more negative onset potential and higher peak current were presented on $Pd_{67}Ag_{33}$ and $Pd_{50}Ag_{50}$ BANWs compared to commercial Pd/C. For Pd NWs and $Pd_{67}Ag_{33}$ and $Pd_{50}Ag_{50}$ BANWs, there is a negative shift of onset potential with the increase of Ag concentration. A higher oxidation peak current is also presented on the sample with more Ag. However, the $Pd_{33}Ag_{67}$ BANW exhibits a more positive onset potential and lower oxidation current peak relative to other 3D NWs. In the backward scan, another oxidation peak is formed on the four CV curves, which is associated with the oxidation of intermediates of ethanol dissociative adsorption. The accumulation of these intermediates will cause "catalyst poisoning".[22,40] The ratio of forward peak current density (I_f) to backward peak current density (I_b) is used to evaluate the catalyst tolerance to carbonaceous intermediates accumulation.[32] The EOR test results show that the I_f/I_b values of the synthesized 3D NWs are larger than that of commercial Pd/C, indicating the better tolerance to carbonaceous intermediates accumulation of as-prepared 3D NWs. Of the four kinds of NWs, $Pd_{50}Ag_{50}$ shows best electrochemical performance for EOR, including more negative onset potential, higher ethanol oxidation peak current, and quite large I_f/I_b value.

To investigate the electrocatalyst stability of 3D Pd NWs, Pd−Ag BANWs, and commercial Pd/C, chronoamperometric tests were carried out on the catalysts at a potential of −0.3 V for 2000 s in N_2-saturated 1 M KOH + 1 M CH_3CH_2OH solution, as shown in Figure 5c. All the catalysts show a significant decay at the very beginning and then remain stable. The current decay of the EOR implies the formation of carbonaceous intermediates, which could poison the active sites of the catalysts. As expected, the $Pd_{50}Ag_{50}$ BANW shows higher

DOI: 10.1021/acsami.5b01963
ACS Appl. Mater. Interfaces 2015, 7, 13842−13848

current density at the start and the end of the tests, indicating its better catalytic activity and stability against the poisoning.[40,41]

Figure 6b shows the TEM image of $Pd_{50}Ag_{50}$ BANWs after scanning the potential between −0.7 and 0.2 V in 1 M KOH + 1 M CH_3CH_2OH solution. It reveals that the NWs' structure was maintained after 20 cycles. The average diameter of the NWs is 7.25 ± 0.5 nm (Figure S1b, Supporting Information), which is close to that before scanning, as shown in Figure 6a. Figure 6c shows the well-dispersed Pd particles supported on carbon materials. However, the Pd particles aggregate together after the test, as shown in Figure 6d. This further confirms the higher stability of Pd−Ag BANWs compared to that of commercial Pd/C catalysts.

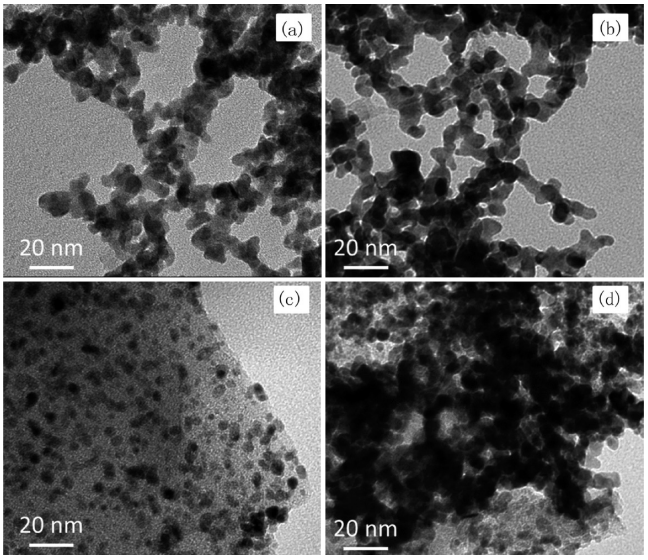

Figure 6. TEM images of $Pd_{50}Ag_{50}$ BANWs before (a) and after (b) 20 potential cycles in 1 M KOH + 1 M CH_3CH_2OH solution. TEM images of commercial Pd/C catalysts before (c) and after (d) 20 potential cycles in 1 M KOH + 1 M CH_3CH_2OH solution.

The enhanced electrochemical catalytic activity and stability of Pd−Ag BANWs toward EOR in alkaline media are attributed to the particular foam-like 3D porous nanostructure as well as the alloy formation between Pd and Ag. Compared with the traditional commercial Pd/C catalyst, which is composed of Pd nanoparticles supported on carbon materials, the self-supported porous 3D BANWs offer numerous advantages to improve the catalytic activity and stability. The 3D porous BANWs do not have to be supported on the high surface carbon materials, which avoids the degradation of carbon materials. On the other hand, 3D porous BANWs are continuous materials with high surface area, which keeps them away from the particle aggregation issue. These advantages ensure the high ECSA, which, in turn, increases the catalytic activity and stability of the materials. On the basis of bifunctional mechanism theory,[40] the Pd−Ag bimetallic alloy is more efficient to remove the carbonaceous intermediates and favorable for the release of the active sites on the catalyst surface. On the other hand, the d-band center of Pd will shift up when combined with Ag atom because of the surface tensile strain which is caused by the difference lattice constant between Ag and Pd.[36,42] Basing on the d-band center theory, a stronger adsorption was formed between Pd−Ag alloy and OH^-, which was favorable for the removal of carbonaceous intermediates, and thus, the oxidation of ethanol on the catalyst surface was improved. However, the more adsorption of OH^- will, in turn, suppress the dissociative adsorption of ethanol.[43] Therefore, the peak current of ethanol electrooxidation decreased in $Pd_{33}Ag_{67}$ BANWs.

In order to evaluate the capability of catalysts to remove the adsorbed poisoning species, the CO stripping experiments on Pd/C, Pd NWs, and $Pd_{50}Ag_{50}$ BANWs were carried out in 1.0 M KOH solution. After purging the solution with N_2 for 30 min, CO was bubbled for 20 min under a fixed potential of −0.3 V vs Ag/AgCl, followed by purging N_2 for another 30 min. The CV curves of CO stripping were recorded at a scanning rate of 50 mV/s. As shown in Figure 7, each sample shows a typical CO oxidation peak in the first cycle. The onset potential of CO oxidation on $Pd_{50}Ag_{50}$ BANWs (−0.35 V) is more negative than that on commercial Pd/C (−0.18 V) and Pd NWs (−0.23 V) catalysts. This indicates the highest ability of $Pd_{50}Ag_{50}$ BANWs to facilitate the removal of CO among the three samples, which also explains the higher catalytic activity of $Pd_{50}Ag_{50}$ BANWs toward ethanol electrooxidation than others. The broad CO oxidation peak on the surface of $Pd_{50}Ag_{50}$ BANWs might be related to the two types of CO_{ads} species on the Pd−Ag surface: Pd adsorbed CO and Ag adsorbed CO.[44] In the second cycle, the CO oxidation peak is not observed on the surface of Pd NWs and $Pd_{50}Ag_{50}$ BANWs, which demonstrates the great ability of the 3D NWs to overcome CO poisoning during EOR.[23]

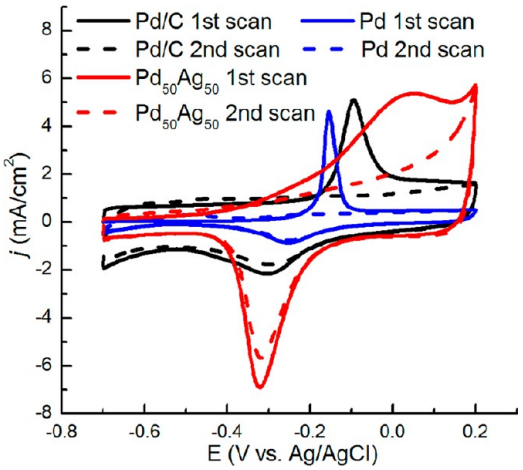

Figure 7. CV curves of CO stripping on commercial Pd/C, Pd NWs, and $Pd_{50}Ag_{50}$ BANWs catalysts. The dash lines are CV curves recorded after CO stripping.

4. CONCLUSIONS

In summary, 3D Pd NWs and Pd−Ag BANWs were synthesized with a fast and simple method on a large scale. The as-synthesized Pd−Ag BANWs presented enhanced electrocatalytic activity and stability toward EOR in alkaline solutions due to the formation of Pd−Ag alloys as well as the porous nanostructures. We demonstrated that the morphology of the 3D NWs was not affected by the composition, while the ratio between Pd and Ag had a significant effect on the electrocatalytic activity toward EOR. Moreover, the Pd−Ag BANWs, with an appropriate composition, exhibited better electrocatalytic activity than that of commercial Pd/C catalyst.

DOI: 10.1021/acsami.5b01963
ACS Appl. Mater. Interfaces 2015, 7, 13842−13848

Therefore, we expect that the well-defined 3D Pd−Ag BANWs could be a promising catalyst for fuel cells.

■ ASSOCIATED CONTENT

Supporting Information

Size distribution of Pd NWs, and $Pd_{67}Ag_{33}$ and $Pd_{50}Ag_{50}$ BANWs. Size distribution of $Pd_{50}Ag_{50}$ BANWs after the test. Element mapping and EDX spectra of $Pd_{67}Ag_{33}$ BANWs. XPS spectra of $Pd_{67}Ag_{33}$ and $Pd_{50}Ag_{50}$ BANWs. The Supporting Information is available free of charge on the ACS Publications website at DOI: 10.1021/acsami.5b01963.

■ AUTHOR INFORMATION

Corresponding Author

*E-mail: yuehe.lin@wsu.edu.

Author Contributions

The manuscript was written through contributions of all authors. All authors have given approval to the final version of the manuscript.

Notes

The authors declare no competing financial interest.

■ ACKNOWLEDGMENTS

This work was supported by a startup fund of Washington State University, USA. We thank Franceschi Microscopy & Image Center at Washington State University for TEM measurements. We would like to acknowledge Dr. Hong-Gang Liao at Lawrence Berkeley National Laboratory for TRTEM measurement.

■ REFERENCES

(1) Zhu, C. Z.; Guo, S. J.; Dong, S. J. PdM (M = Pt, Au) Bimetallic Alloy Nanowires with Enhanced Electrocatalytic Activity for Electrooxidation of Small Molecules. *Adv. Mater.* **2012**, *24* (17), 2326−2331.

(2) Wang, F.; Li, C. H.; Sun, L. D.; Xu, C. H.; Wang, J. F.; Yu, J. C.; Yan, C. H. Porous Single-Crystalline Palladium Nanoparticles with High Catalytic Activities. *Angew. Chem., Int. Ed.* **2012**, *51* (20), 4872−4876.

(3) Liu, Z. Y.; Yang, L.; Liu, L.; Chong, X. Y.; Guo, J.; Ma, S. H.; Ji, Y. H.; He, Y. H. Parallel-Scan Based Microarray Imager Capable of Simultaneous Surface Plasmon Resonance and Hyperspectral Fluorescence Imaging. *Biosens. Bioelectron.* **2011**, *30* (1), 180−187.

(4) Liu, Z. Y.; Liu, L.; Wang, X. X.; Shi, H.; Chong, X. Y.; Ma, S. H.; Ji, Y. H.; Guo, J. H.; Ma, H.; He, Y. H. Polarization-Interferometry-Based Wavelength-Interrogation Surface Plasmon Resonance Imager for Analysis of Microarrays. *J. Biomed. Opt.* **2012**, *17* (3), 0360021−0360028.

(5) Chong, X. Y.; Liu, L.; Liu, Z. Y.; Ma, S. H.; Guo, J.; Ji, Y. H.; He, Y. H. Detect the Hybridization of Single-Stranded DNA by Parallel Scan Spectral Surface Plasmon Resonance Imaging. *Plasmonics* **2013**, *8* (2), 1185−1191.

(6) Yi, S. J.; Sun, L. M.; Lenaghan, S. C.; Wang, Y. Z.; Chong, X. Y.; Zhang, Z. L.; Zhang, M. J. One-Step Synthesis of Dendritic Gold Nanoflowers with High Surface-Enhanced Raman Scattering (SERS) Properties. *R. Soc. Chem. Adv.* **2013**, *3* (26), 10139−10144.

(7) Yang, J.; R, F.; Chong, X.; Fan, D.; Chakravarty, S.; Wang, Z.; Chen, R.; Wang, A. Guided-Mode Resonance Grating with Self-Assembled Silver Nanoparticles for Surface-Enhanced Raman Scattering Spectroscopy. *Photonics* **2014**, *1* (4), 380−389.

(8) Liu, L.; Ma, S. H.; Ji, Y. H.; Chong, X. Y.; Liu, Z. Y.; He, Y. H.; Guo, J. H. A Two-Dimensional Polarization Interferometry Based Parallel Scan Angular Surface Plasmon Resonance Biosensor. *Rev. Sci. Instrum.* **2011**, *82* (2), 023109.

(9) Moon, G. D.; Choi, S. W.; Cai, X.; Li, W. Y.; Cho, E. C.; Jeong, U.; Wang, L. V.; Xia, Y. N. A New Theranostic System Based on Gold Nanocages and Phase-Change Materials with Unique Features for Photoacoustic Imaging and Controlled Release. *J. Am. Chem. Soc.* **2011**, *133* (13), 4762−4765.

(10) Li, W. Y.; Cai, X.; Kim, C. H.; Sun, G. R.; Zhang, Y.; Deng, R.; Yang, M. X.; Chen, J. Y.; Achilefu, S.; Wang, L. V.; Xia, Y. N. Gold Nanocages Covered with Thermally-Responsive Polymers for Controlled Release by High-Intensity Focused Ultrasound. *Nanoscale* **2011**, *3* (4), 1724−1730.

(11) Evarts, S. E.; Kendrick, I.; Wallstrom, B. L.; Mion, T.; Abedi, M.; Dimakis, N.; Smotkin, E. S. Ensemble Site Requirements for Oxidative Adsorption of Methanol and Ethanol on Pt Membrane Electrode Assemblies. *ACS Catal.* **2012**, *2* (5), 701−707.

(12) Li, M.; Liu, P.; Adzic, R. R. Platinum Monolayer Electrocatalysts for Anodic Oxidation of Alcohols. *J. Phys. Chem. Lett.* **2012**, *3* (23), 3480−3485.

(13) Ramulifho, T.; Ozoemena, K. I.; Modibedi, R. M.; Jafta, C. J.; Mathe, M. K. Fast Microwave-Assisted Solvothermal Synthesis of Metal Nanoparticles (Pd, Ni, Sn) Supported on Sulfonated MWCNTs: Pd-Based Bimetallic Catalysts for Ethanol Oxidation in Alkaline Medium. *Electrochim. Acta* **2012**, *59*, 310−320.

(14) Oliveira, M. C.; Rego, R.; Fernandes, L. S.; Tavares, P. B. Evaluation of the Catalytic Activity of Pd-Ag Alloys on Ethanol Oxidation and Oxygen Reduction Reactions in Alkaline Medium. *J. Power Sources* **2011**, *196* (15), 6092−6098.

(15) Jiang, H. L.; Zhu, Y. H.; Feng, Q.; Su, Y. H.; Yang, X. L.; Li, C. Z. Nitrogen and Phosphorus Dual-Doped Hierarchical Porous Carbon Foams as Efficient Metal-Free Electrocatalysts for Oxygen Reduction Reactions. *Chem.—Eur. J.* **2014**, *20* (11), 3106−3112.

(16) Zhao, Y. C.; Zhan, L.; Tian, J. N.; Nie, S. L.; Ning, Z. Enhanced Electrocatalytic Oxidation of Methanol on Pd/Polypyrrole-Graphene in Alkaline Medium. *Electrochim. Acta* **2011**, *56* (5), 1967−1972.

(17) Konopka, D. A.; Li, M.; Artyushkova, K.; Marinkovic, N.; Sasaki, K.; Adzic, R.; Ward, T. L.; Atanassov, P. Platinum Supported on NbRuyOz as Electrocatalyst for Ethanol Oxidation in Acid and Alkaline Fuel Cells. *J. Phys. Chem. C* **2011**, *115* (7), 3043−3056.

(18) Erini, N.; Loukrakpam, R.; Petkov, V.; Baranova, E. A.; Yang, R. Z.; Teschner, D.; Huang, Y. H.; Brankovic, S. R.; Strasser, P. Ethanol Electro-Oxidation on Ternary Platinum-Rhodium-Tin Nanocatalysts: Insights in the Atomic 3D Structure of the Active Catalytic Phase. *ACS Catal.* **2014**, *4* (6), 1859−1867.

(19) Yu, F. J.; Zhou, W. Z.; Bellabarba, R. M.; Tooze, R. P. One-Step Synthesis and Shape-Control of CuPd Nanowire Networks. *Nanoscale* **2014**, *6* (2), 1093−1098.

(20) Du, W. X.; Mackenzie, K. E.; Milano, D. F.; Deskins, N. A.; Su, D.; Teng, X. W. Palladium-Tin Alloyed Catalysts for the Ethanol Oxidation Reaction in an Alkaline Medium. *ACS Catal.* **2012**, *2* (2), 287−297.

(21) Shih, Z. Y.; Wang, C. W.; Xu, G. B.; Chang, H. T. Porous Palladium Copper Nanoparticles for the Electrocatalytic Oxidation of Methanol in Direct Methanol Fuel Cells. *J. Mater. Chem. A* **2013**, *1* (15), 4773−4778.

(22) Zhu, C. Z.; Guo, S. J.; Dong, S. J. Rapid, General Synthesis of PdPt Bimetallic Alloy Nanosponges and Their Enhanced Catalytic Performance for Ethanol/Methanol Electrooxidation in an Alkaline Medium. *Chem.—Eur. J.* **2013**, *19* (3), 1104−1111.

(23) Ding, L. X.; Wang, A. L.; Ou, Y. N.; Li, Q.; Guo, R.; Zhao, W. X.; Tong, Y. X.; Li, G. R. Hierarchical Pd-Sn Alloy Nanosheet Dendrites: An Economical and Highly Active Catalyst for Ethanol Electrooxidation. *Sci. Rep.* **2013**, *3*, 1181.

(24) Hong, W.; Wang, J.; Wang, E. K. Synthesis of Porous PdAg Nanoparticles with Enhanced Electrocatalytic Activity. *Electrochem. Commun.* **2014**, *40*, 63−66.

(25) Yin, Z.; Zheng, H. J.; Ma, D.; Bao, X. H. Porous Palladium Nanoflowers that Have Enhanced Methanol Electro-Oxidation Activity. *J. Phys. Chem. C* **2009**, *113* (3), 1001−1005.

(26) Lu, Y. Z.; Chen, W. Nanoneedle-Covered Pd-Ag Nanotubes: High Electrocatalytic Activity for Formic Acid Oxidation. *J. Phys. Chem. C* **2010**, *114* (49), 21190−21200.

DOI: 10.1021/acsami.5b01963
ACS Appl. Mater. Interfaces 2015, 7, 13842−13848

(27) Kim, K.-J.; Chong, X.; Kreider, P. B.; Ma, G.; Ohodnicki, P. R.; Baltrus, J. P.; Wang, A. X.; Chang, C.-H. Plasmonics-Enhanced Metal-Organic Framework Nanoporous Films for Highly Sensitive Near-Infrared Absorption. *J. Mater. Chem. C* **2015**, *3* (12), 2763−2767.
(28) Jung, S. M.; Jung, H. Y.; Dresselhaus, M. S.; Jung, Y. J.; Kong, J. A Facile Route for 3D Aerogels from Nanostructured 1D and 2D Materials. *Sci. Rep.* **2012**, *2*, 849.
(29) Xiao, S.; Xiao, F.; Hu, Y.; Yuan, S. L.; Wang, S.; Qian, L. H.; Liu, Y. Q. Hierarchical Nanoporous Gold-Platinum with Heterogeneous Interfaces for Methanol Electrooxidation. *Sci. Rep.* **2014**, *4*, 4370.
(30) Sun, S. H.; Zhang, G. X.; Geng, D. S.; Chen, Y. G.; Li, R. Y.; Cai, M.; Sun, X. L. A Highly Durable Platinum Nanocatalyst for Proton Exchange Membrane Fuel Cells: Multiarmed Starlike Nanowire Single Crystal. *Angew. Chem., Int. Ed.* **2011**, *50* (2), 422−426.
(31) Yang, S. C.; Luo, X. Mesoporous Nano/micro Noble Metal Particles: Synthesis and Applications. *Nanoscale* **2014**, *6* (9), 4438−4457.
(32) Peng, C.; H, Y.; Liu, M.; Zheng, Y. Hollow Raspberry-like PdAg Alloy Nanospheres: High Electrocatalytic Activity for Ethanol Oxidation in Alkaline Media. *J. Power Sources* **2015**, *278*, 69−75.
(33) Kakaei, K.; Dorraji, M. One-pot Synthesis of Palladium Silver Nanoparticles Decorated Reduced Graphene Oxide and Their Application for Ethanol Oxidation in Alkaline Media. *Electrochim. Acta* **2014**, *143*, 207−215.
(34) Pan, H. B.; Wai, C. M. Facile Sonochemical Synthesis of Carbon Nanotube-supported Bimetallic Pt-Rh Nanoparticles for Room Temperature Hydrogenation of Arenes. *New J. Chem.* **2011**, *35*, 1649−1660.
(35) Liu, W.; Rodriguez, P.; Borchardt, L.; Foelske, A.; Yuan, J. P.; Herrmann, A. K.; Geiger, D.; Zheng, Z. K.; Kaskel, S.; Gaponik, N.; Kotz, R.; Schmidt, T. J.; Eychmuller, A. Bimetallic Aerogels: High-Performance Electrocatalysts for the Oxygen Reduction Reaction. *Angew. Chem., Int. Ed.* **2013**, *52* (37), 9849−9852.
(36) Nguyen, S. T.; Law, H. M.; Nguyen, H. T.; Kristian, N.; Wang, S. Y.; Chan, S. H.; Wang, X. Enhancement Effect of Ag for Pd/C towards the Ethanol Electro-oxidation in Alkaline Media. *Appl. Catal., B* **2009**, *91* (1−2), 507−515.
(37) Qiu, Y.; Xin, L.; Chadderdon, D. J.; Qi, J.; Liang, C. H.; Li, W. Z. Integrated Electrocatalytic Processing of Levulinic Acid and Formic Acid to Produce Biofuel Intermediate Valeric Acid. *Green Chem.* **2014**, *16* (3), 1305−1315.
(38) Zhang, Q. L.; Feng, J. X.; Wang, A. J.; Wei, J.; Feng, J. J. Simple Synthesis of Bimetallic Alloyed Pd-Au Nanochain Networks Supported on Reduced Graphene Oxide for Enhanced Oxygen Reduction Reaction. *RSC Adv.* **2014**, *4* (95), 52640−52646.
(39) Kibsgaard, J.; Gorlin, Y.; Chen, Z. B.; Jaramillo, T. F. Meso-Structured Platinum Thin Films: Active and Stable Electrocatalysts for the Oxygen Reduction Reaction. *J. Am. Chem. Soc.* **2012**, *134* (18), 7758−7765.
(40) Liang, Z. X.; Zhao, T. S.; Xu, J. B.; Zhu, L. D. Mechanism Study of the Ethanol Oxidation Reaction on Palladium in Alkaline Media. *Electrochim. Acta* **2009**, *54* (8), 2203−2208.
(41) Hu, G. Z.; Nitze, F.; Barzegar, H. R.; Sharifi, T.; Mikolajczuk, A.; Tai, C. W.; Borodzinski, A.; Wagberg, T. Palladium Nanocrystals Supported on Helical Carbon Nanofibers for Highly Efficient Electro-oxidation of Formic Ccid, Methanol and Ethanol in Alkaline Electrolytes. *J. Power Sources* **2012**, *209*, 236−242.
(42) Hammer, B.; Norskov, J. K. Theoretical Surface Science and Catalysis - Calculations and Concepts. *Adv. Catal.* **2000**, *45*, 71−129.
(43) Bianchini, C.; Shen, P. K. Palladium-Based Electrocatalysts for Alcohol Oxidation in Half Cells and in Direct Alcohol Fuel Cells. *Chem. Rev.* **2009**, *109* (9), 4183−4206.
(44) Liu, Z. F.; Jackson, G. S.; Eichhorn, B. W. PtSn Intermetallic, Core-Shell, and Alloy Nanoparticles as CO-Tolerant Electrocatalysts for H_2 Oxidation. *Angew. Chem., Int. Ed.* **2010**, *49* (18), 3173−3176.

DOI: 10.1021/acsami.5b01963
ACS Appl. Mater. Interfaces 2015, 7, 13842−13848